Journal of Solid State Chemistry 198 (2013) 39–44

Contents lists available at SciVerse ScienceDirect

Journal of Solid State Chemistry

journal homepage: www.elsevier.com/locate/jssc

Novel alkaline earth copper germanates with ferro and antiferromagnetic $S=1/2$ chains

Paula Brandão [a], Mario S. Reis [b], Zheng Gai [c], António M. dos Santos [d,*]

[a] CICECO, Universidade de Aveiro, 3810-193 Aveiro, Portugal
[b] Instituto de Física, Universidade Federal Fluminense, Av. Gal. Milton Tavares de Souza s/n, 24210-346 Niterói-RJ, Brazil
[c] Center for Nanophase Materials Sciences, Oak Ridge National Laboratory Oak Ridge, TN 37831-6487, USA
[d] Quantum Condensed Matter Division, Neutron Sciences Directorate, Oak Ridge National Laboratory Oak Ridge, TN 37831-6460, USA

ARTICLE INFO

Article history:
Received 11 April 2012
Received in revised form
16 June 2012
Accepted 4 September 2012
Available online 23 September 2012

Keywords:
Hydrothermal synthesis
Crystal structure
Copper germanates
Magnetic chains

ABSTRACT

Two new alkaline earth copper(II) germanates were hydrothermally synthesized: $CaCuGeO_4 \cdot H_2O$ (**1**) and $BaCu_2Ge_3O_9 \cdot H_2O$ (**2**), and their structures determined by single crystal X-ray diffraction. Compound (**1**) crystallizes in space group $P2_1/c$ with $a=5.1320(2)$ Å, $b=16.1637(5)$ Å, $c=5.4818(2)$ Å, $\beta=102.609(2)^\circ$, $V=443.76(3)$ Å^3 and $Z=4$. This copper germanate contains layers of composition $[CuGeO_4]^{2-}_{\infty}$ comprising CuO_4 square planes and GeO_4 tetrahedra with calcium and water molecules in the inter-layer space. Compound (**2**) crystallizes in the *Cmcm* space group with $a=5.5593(3)$ Å, $b=10.8606(9)$ Å, $c=13.5409(8)$ Å, $V=817.56(9)$ Å^3 and $Z=4$. This structure contains GeO_6 and CuO_6 octahedra as well as GeO_4 tetrahedra, forming a three-dimensional network of interconnecting six-membered ring channels. The magnetic susceptibility for both samples can be interpreted as $S=1/2$ chains, in agreement with the copper topology observed in the crystal structure. The susceptibility of (**1**) exhibits a Bonner–Fisher type behavior, resulting from antiferromagnetic intra-chain interactions without three-dimensional ordering down to 5 K—the lowest measured temperature. This observation, together with the absence of super-exchange paths between the copper chains, make this system particularly promising for the study of low dimensional magnetism. The magnetic properties of (**2**) show a very weak ferromagnetic near-neighbor interaction along the chain. In this compound a peak the χT plot seems to indicate the onset of interchain antiferromagentic correlations. However, no ordering temperature is detected in the susceptibility data.

Published by Elsevier Inc.

1. Introduction

The search for new topologically complex oxides with open framework has been extremely intensive because of their interesting properties in catalysis, molecular sieves, gas storage and other important technological applications [1]. In that context, zeolite type materials, formed by SiO_4 and AlO_4 corner sharing tetrahedra, and their substitution for other elements with different coordinations, has attracted tremendous research [2–4]. By contrast, open framework germanate compounds are much less explored. Unlike silicon oxides that primarily form SiO_4 tetrahedra, germanium framework oxides can exhibit GeO_4 tetrahedra, GeO_5 trigonal bipyramids and GeO_6 octahedra. As a result, a wide variety of germanium compounds, consisting of both purely tetrahedrally coordinated framework and mixed polyhedral frameworks have been reported [5,6]. Profiting from this structural variability, it is possible, through the incorporation of magnetically active ions to germanium based frameworks, to obtain of novel magnetic materials with a wide variety of structural building blocks, including chains, layered systems and three-dimensional networks, where the observed magnetic behavior is often mapped on the crystal structure topology. Illustrating this point, there are some recent examples of open framework transition metal (nickel and cobalt) germanates [7,8]. The use of copper in these structurally diverse environments is particularly advantageous as its spin $S=1/2$, in the conventional 2+ oxidation state, results in systems with quantum magnetism. Examples of this are $CuGeO_3$ (linear chain) [9], $CaCuGe_2O_6$ (isolated dimer) [10], $BaCu_2Ge_2O_7$ (zigzag chain) [11] or di-copper tetra-carboxylate (quantum entanglement) [12]. It is also widely recognized that the use of soft chemistry methods is an efficient strategy to obtain novel materials, exhibiting various interesting magnetic phenomena, as these synthesis methods often result in systems with complex geometries.

To the best of our knowledge, there are only few copper germanate complex framework structures published: an organically

* Corresponding author.
E-mail address: dossantosam@ornl.gov (A.M. dos Santos).

0022-4596/$ - see front matter Published by Elsevier Inc.
http://dx.doi.org/10.1016/j.jssc.2012.09.006

Table 1
Structural parameters of selected open framework copper germanates.

Composition	Space group	Unit cell volume (Å^3)	Building blocks	Refs.
$BaCu_2Ge_2O_7$	*Pnma*	663.52(14)	GeO_4, CuO_4; $d_{Cu-Cu}=3.556(1)$ Å; corner sharing Cu–O	[11]
$CaCuGe_2O_6$	$P2_1/c$	468.16(15)	GeO_4, GeO_5, CuO_4; $d_{Cu-Cu}=3.064(2)$ Å; edge sharing Cu–O	[10]
$K_2Cu_3Ge_5O_{14}$	$P\bar{1}$	324.55(4)	GeO_4, GeO_6 CuO_4, CuO_5; $d_{Cu-Cu}=2.793(9)$–$2.833(2)$ Å; edge sharing Cu–O	[13]

templated sodium copper germanate [14], and others synthesized at higher temperature [10,11,13]. The crystallographic and structural information of these compounds is summarized in Table 1 in order to illustrate their topological richness.

Here we report the synthesis, crystal structure determination and magnetic characterization of two novel copper (II) germanates: a three-dimensional $BaCu_2Ge_3O_9 \cdot H_2O$, and a layered $CaCuGeO_4 \cdot H_2O$, both prepared hydrothermally under mild conditions.

2. Experimental details

Samples were prepared via hydrothermal synthesis under autogeneous pressure and basic conditions, yielding purple single crystals for (**1**) and green plate crystals for (**2**). Powder diffraction measurements of the reaction products indicated that, in addition to the crystals collected for structure determination, sodium germanate (Na_2GeO_3) was also present as a fine powder.

Synthesis of $CaCuGeO_4 \cdot H_2O$ (**1**): A typical synthesis was made by mixing 26.31 g H_2O and 3.80 g $Cu(SO_4) \cdot 5H_2O$ (Pronalab). A second solution was obtained by mixing 12.83 g H_2O, 2.30 g $Ca(OH)_2$ (Merck) and 1.50 g GeO_2 (Aldrich). These two solutions were combined and stirred thoroughly until a homogeneous gel was obtained. This mixture was sealed in teflon lined autoclaves and heated at 230 °C for 7 days.

Synthesis of $BaCu_2Ge_3O_9 \cdot H_2O$ (**2**): A typical synthesis was made by mixing 18.45 g H_2O and 3.58 g $Cu(SO_4) \cdot 5H_2O$ (Pronalab). A second solution was obtained by mixing 18.07 g H_2O, 6.07 g $Ba(OH)_2 \cdot 8H_2O$ (Aldrich) and 1.50 g GeO_2 (Aldrich). These two solutions were combined and stirred thoroughly until a homogeneous gel was obtained. The resulting gel was sealed in teflon lined autoclaves and heated at 230 °C for 7 days.

These autoclaves were cooled in air and the reaction products were washed and filtered to collect the resulting crystals, that were dried at room temperature. Susceptibility measurements were performed on polycrystalline samples on a *Quantum Design* superconducting quantum interference device—SQUID—magnetometer. Data were collected upon heating, from 5 K to 300 K using an excitation field of 1000 Oe on samples cooled in the absence of magnetic field (ZFC).

2.1. Structure determination and refinement

Single crystal X-ray data were collected on a Bruker APEX II CCD area detector, using graphite monochromatized Mo$K\alpha$ radiation ($\lambda=0.71073$ Å) with the sample placed at 35 mm from the detector. Each frame was measured for a counting time of 50 s for (**1**) and 80 s for (**2**). Data were collected with the samples cooled to 150(2) K. Data reduction and multi-scan correction for absorption effects were carried out using the SAINT-NT software package from Bruker AXS. The structures were solved by means of direct methods, using SHELXS [15,16] followed of subsequent difference Fourier syntheses. The resulting structures were then refined using full-matrix least squares in SHELXL [15,16].

Table 2
Crystallographic data and structure refinement parameters for $BaCu_2Ge_3O_9 \cdot H_2O$ and $CaCuGeO_4 \cdot H_2O$.

Empirical formula	$BaCu_2Ge_3O_9 \cdot H_2O$	$CaCuGeO_4 \cdot H_2O$
Formula weight	644.21	258.23
Unit cell		
Crystal system	Orthorhombic	Monoclinic
Space group	*Cmcm*	$P2_1/c$
a (Å)	5.5593(3)	5.1320(2)
b (Å)	10.8606(9)	16.1637(5)
c (Å)	13.5409(8)	5.4818(2)
α (°)	90	90
β (°)	90	102.609(2)
γ (°)	90	90
V (Å^3)	817.56(9)	443.76 (3)
Z	4	4
D_{calc} (g cm^{-3})	5.234	3.865
Experimental parameters		
Absorpt. correct. (mm^{-1})	20.782	12.632
Crystal size (mm)	$0.02\times0.02\times0.01$	$0.01\times0.01\times0.01$
θ range (°)	3.75–25.64	4.01–30.58
Reflections collected	4773	4939
Unique reflections, R_{int}	446, 0.0593	1353, 0.0361
Final R indices		
$R1$, wR_2 [$I_0>2\sigma(I_0)$]	0.0247, 0.0546	0.0243, 0.0521
$R1$, wR_2 [all data]	0.0340, 0.0569	0.0323, 0.0545

$R1=\Sigma[|F_o|-|F_c|]/\Sigma|F_0|$; $wR_2=\Sigma[w[|F_o|-|F_c|]^2/\Sigma w[|F_o|^2]^{1/2}$.

The atomic positions of hydrogen atoms of the water molecules were directly obtained from the last difference Fourier maps. Anisotropic thermal parameters were used for all non-hydrogen atoms, while the hydrogen atoms of the water molecules were refined with isotropic parameters equivalent to 1.2 times those of the atom to which they are bonded. The crystal data and refinement details are given in Table 2. Molecular diagrams were drawn with the *Vesta* software suite [17].

3. Results

3.1. Crystal structures

3.1.1. Crystal structure of $CaCuGeO_4 \cdot H_2O$

The asymmetric unit of (**1**) contains two independent copper centers Cu(1) and Cu(2), both located on an inversion center, one GeO_4 tetrahedra, one Ca cation and one hydrogen bonded water molecule. This copper germanate comprises layers of composition $[CuGeO_4]^{2-}_{\infty}$ containing CuO_4 and GeO_4 tetrahedra separated by calcium and the water molecules (Fig. 1). The two independent copper centers exhibit square planar geometry (Fig. 2, bottom), the copper site Cu(1) is surrounded by four oxygen atoms with Cu(1)–O distances of 1.922(2) Å and 1.967(2) Å, and the O–Cu(1)–O bond angles of 87.72(8)° and 92.28(8)°.

The second copper site Cu(2) is coordinated also with four oxygen atoms with Cu(2)–O distances of 1.917(2) and 1.971(2) Å and the O–Cu(2)–O bond angles of 88.63(8)° and 91.37(8)°. Both CuO_4 squares share corners, forming an infinite chain of

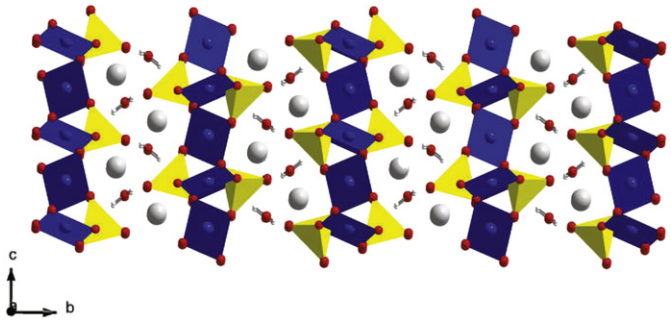

Fig. 1. The structure of (**1**) viewed along the *a* direction showing the two-dimensional $[CuGeO_4]^{2-}_{\infty}$ layers. Color scheme: Cu, blue polyhedra; Ge, yellow polyhedra; O, red; H, white; Ca, gray. (For interpretation of the references to color in this figure caption, the reader is referred to the web version of this article.)

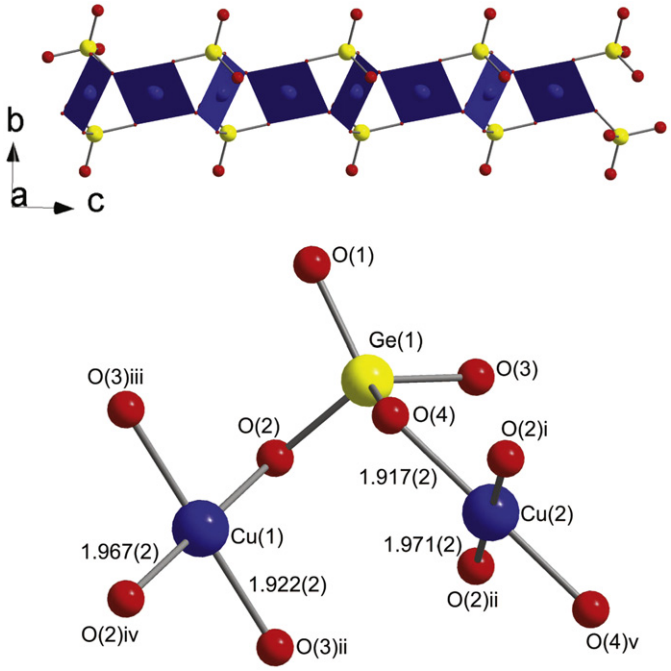

Fig. 2. (Top): Mixed ball-and-stick and polyhedral representation of the square-planar Cu chain. (Bottom): The coordination environment of Cu(1) and Cu(2) metal centers in (**1**). Color scheme: Cu, blue ; Ge, yellow; O, red; H, white. Coordinates of equivalent atomic positions: (i) x, y, $1+z$; (ii) $-x$, $1-y$, $-z$; (iii) $1+x$, y, z; (iv) $1-x$, $1-y$, $-z$; (viii) $-x$, $1-y$, $1-z$. (For interpretation of the references to color in this figure caption, the reader is referred to the web version of this article.)

Cu–O–Cu, running along the [101] direction, with a metal-to-metal distance of 3.3204(7) Å and a Cu–O–Cu angle of 115.2(3)° (Fig. 2, top). The Ge–O bond distances vary from 1.741(2) to 1.784(2) Å and are comparable with other compounds which contain germanium in tetrahedral coordination. [10,11,13] The O-Ge-O angles are distributed in the range of 101.96(9)-112.57(9)°. The calcium cations and the water molecules are located between layers. These layers are connected through hydrogen bonds between the water molecule O(100) and the O(1) and O(3) oxygens atoms from the GeO_4 tetrahedra. Additional structural details on the hydrogen bonding scheme is presented in Supplemental information.

3.1.2. *Crystal structure of* $BaCu_2Ge_3O_9 \cdot H_2O$

The barium germanate (**2**), crystallizes in the orthorhombic space group *Cmcm* with $Z=4$. The open framework structure shown in Fig. 3 can be viewed as being formed of layers of CuO_6, GeO_4 and GeO_6 interconnected via GeO_4 tetrahedra forming two types of six member rings channels. One, running along the *a* axis, contains four GeO_4 and two CuO_6 sharing all the corners presenting an aperture of 6.1×4.3 Å (Fig. 3, left). The channels running along the *b* axis are formed by four GeO_4 and two GeO_6 corner-linked units showing an aperture of 5.6×4.3 Å (Fig. 3 right). A peculiarity in this structure is that the bridging oxygen between the layers—O(4), is only double coordinated, with a Ge(1)–O(4)–Ge(1) angle of 173.8° (as can be seen in the left panel of Fig. 3) this causes a slight instability about the Ge–O(4)–Ge axis, that is reflected in an anomalously high ADP for that atom. The octahedral coordination around the Cu atom, represented in the top panel of Fig. 4 is strongly Jahn–Teller distorted due to the effect of the Cu^{2+} ion, which has four short Cu–O bonds 1.909(5)–1.991(4) Å, and two long Cu–O bonds of 2.475(5) Å. This octahedra has two Cu–O–Cu angles in the equatorial plane, 87.01(18)° and 92.99(18)°. The octahedral environment is further distorted by the apical oxygen (O3) not being perpendicular to the equatorial plane, but being tilted by about 16° making one of the O_{ap}–O_{eq} bonds long—3.146(7) Å and the other short 2.663(7) Å (see inset of Fig. 4). These octahedra share edges forming an infinite chain of Cu–O–Cu (Fig. 4, bottom) running along the *a* direction, in which the metal-to-metal distance is of 2.779(7) Å, comparable to $K_2Cu_3Ge_5O_{14}$ [13]. It is interesting to note that the equatorial plane of consecutive octahedra are buckled with an angle of 158° (see inset of Fig. 4). The average Ge–O bond length for the GeO_4 tetrahedra is 1.715(3) Å. The germanium octahedron is nearly regular, as it has four Ge–O bond lengths of 1.944(5) Å and two Ge–O distances of 1.822(7) Å. These distances compare well with those found in other related copper samples with

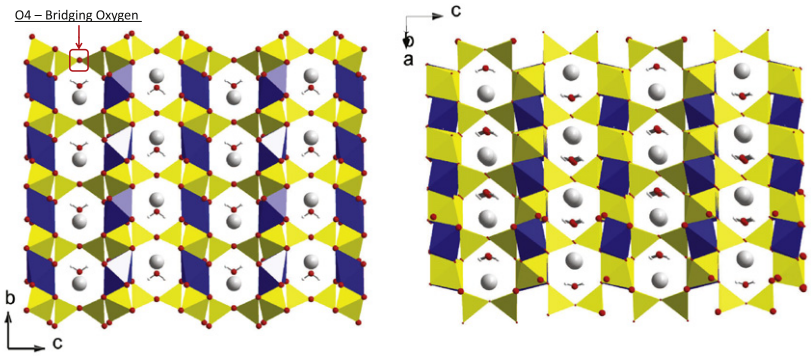

Fig. 3. Crystal structure of (**2**). (Left) Viewed along *a* axis showing the six member ring formed by four GeO_4 tetrahedra and two CuO_6 octahedra. (Right) View along the *b* axis showing the six member rings formed by four GeO_4 tetrahedra and two GeO_6 octahedra. Color scheme: Cu, blue polyhedra; Ge, yellow polyhedra; O, red; H, white; Ba, gray. (For interpretation of the references to color in this figure caption, the reader is referred to the web version of this article.)

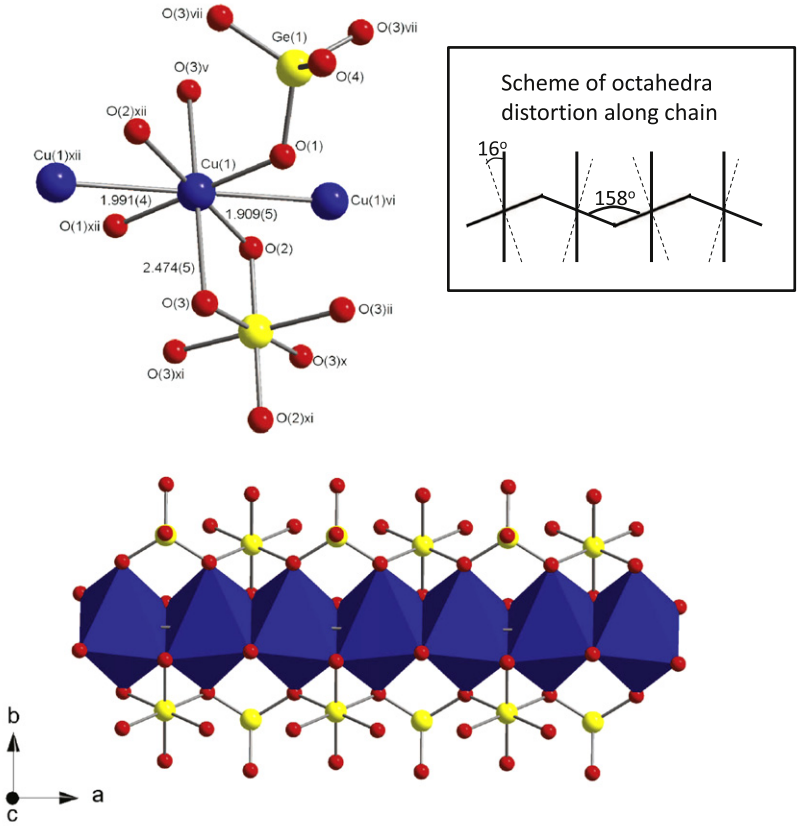

Fig. 4. Top: The coordination environment of Cu(II) in compound (**2**). Bottom: Mixed ball-and-stick and polyhedral representation of the Cu chain running along the *a* direction. Inset: CuO_4 tilting along the chain and angle between apical oxygen and equatorial plane. Color scheme: Cu, blue polyhedra; Ge, yellow ; O, red. Coordinates of equivalent atomic positions: (v) $0.5-x$, $0.5-y$, $1-z$; (vi) $-0.5+x$, $0.5-y$, $1-z$; (xii) $0.5+x$, $0.5-y$. (For interpretation of the references to color in this figure caption, the reader is referred to the web version of this article.)

germanium [10,11,13]. The barium cations and water molecules are located within the six member-ring channels and barium is coordinated with six oxygen atoms in a regular octahedral coordination where the average Ba–O is 2.758(3) Å. The water molecule resides inside the channels and is hydrogen bonded to the framework (see Supplemental information for additional structural details on the hydrogen bonding).

3.2. Magnetic properties

Clues for the interpretation of the magnetic data collected in these compounds can be inferred from an inspection of their crystal structure, in particular the copper first coordination shell and Cu–Cu connectivity. In fact, while both structures contain copper ions in a chain arrangement, their magnetic behavior is significantly different, as can be seen in the plot of their inverse susceptibility, shown in Fig. 5.

The topological case that can be applied to model both crystal structures is a $S=1/2$ equally spaced (single exchange parameter J) infinite chain. The $S=1/2$ arises from the Cu^{2+} in d^9 configuration, and the single exchange as there is only one magnetic super-exchange path connecting neighboring copper ions along the chain. To account for all the contributions to the experimental data, it is necessary to add to the chain magnetic susceptibility (χ_c) two additional terms: one related to a temperature independent contribution χ_{ti} and a Curie–Weiss term ρ accounting for paramagnetic species that contaminate the bulk sample. Thus, the total susceptibility can be written as

$$\chi = \rho\frac{C}{T} + (1-\rho)\chi_c + \chi_{ti} \quad (1)$$

where the Curie constant is

$$C = \frac{g^2\mu_B^2}{4k_B} \quad (2)$$

The reciprocal susceptibility, χ^{-1} plotted with the temperature independent contribution subtracted from the data (see Table 3) is presented in Fig. 5. At high temperature, both compounds present a paramagnetic-like behavior. The paramagnetic effective moment $p_{eff} = g\sqrt{J(J+1)}$ (where J, the total angular moment, is $J=L+S$), and the paramagnetic Curie temperature θ_p can be extracted from these data and their values are presented in Table 3. The observed paramagnetic effective moment is close to the theoretical value of $p_{eff} = 1.73\mu_B$/Cu for $S=1/2$, $L=0$, and $g=2$. The small deviations from the ideal value are due to a not fully quenched orbital moment. The extracted θ_p obtained from the extrapolation of the high temperature inverse susceptibility yields a strong negative value of θ_p for (**1**), and a very small positive one for (**2**). Those observations are in good qualitative agreement with the Goodenough–Kanamori rules [18,19] that predict that the magnetic exchange between corner shared octahedra is "strongly" antiferromagentic, while between edge shared octahedra is "weakly" ferromagnetic.

The preliminary determination of the sign of the magnetic exchange is important because, although there is no analytical solution to model the magnetic susceptibility of an infinite,

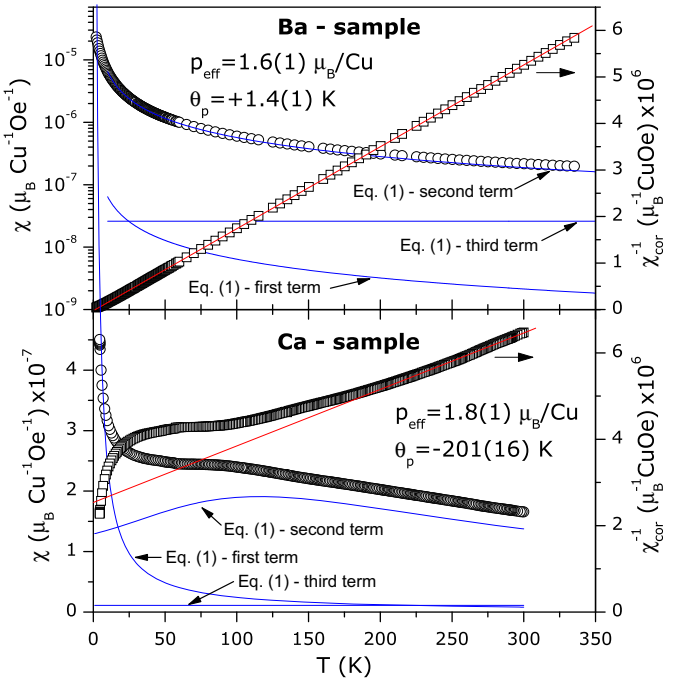

Fig. 5. Susceptibility (left) and its inverse (right) for both barium and calcium containing samples.

Table 3
Relevant parameters for (**1**) and (**2**) obtained from fits of the high temperature data to a Curie–Weiss law (see Fig. 5).

Sample	p_{eff} (μ_B/Cu)	θ_p (K)	χ_{ti} (μ_B/Cu-Oe)
$CaCuGeO_4 \cdot H_2O$	1.8(1)	−201(16)	$+4.69 \times 10^{-9}$
$BaCu_2Ge_3O_9 \cdot H_2O$	1.6(1)	+1.4(1)	$+2.89 \times 10^{-8}$

Table 4
Fits of (**1**) and (**2**) to a regular $S=1/2$ chain.

Sample	J (K)	ρ (%)
$CaCuGeO_4 \cdot H_2O$	−185(3)	4.0(2)
$BaCu_2Ge_3O_9 \cdot H_2O$	+0.8(1)	2.5(2)

equally spaced, chain, in the particular the case of $S=1/2$, a numerical solution was obtained for the antiferromagnetic case ($J<0$) by Bonner and Fisher [20] and for a ferromagnetic arrangement ($J>0$) by Baker and co-workers [21,22]. The mathematical expressions and corresponding numerical parameters are presented in the Supplemental Information, and the results of the fits of the data to the appropriate expression are presented in Table 4, where only J and ρ were refined and was kept at $g=2$ (the ideal value for $L=0$).

For (**1**), where $J<0$, the direct observation of the characteristic maximum of the Bonner-Fisher susceptibility is precluded by the presence of 4% paramagnetic impurities. However, by plotting separately the different terms of the fitted susceptibility of Fig. 5 it is possible to observe that a broad maximum occurs at a temperature of ca. 115 K. This is in agreement with the Bonner–Fisher model [23] that predicts a maximum in the susceptibility in the vicinity of $T_{max}=0.641 \times |J|$, well in line with the resulting value of $J=-185$ K. Topologically, this system is rather similar to the recently reported $AgCuVO_4$, that contains square planar copper with non-magnetic VO_4 tetrahedra, that also exhibits a quasi-one-dimensional chain behavior [24]. Interestingly in that case, the magnitude of the intra-chain magnetic exchange is far greater ($J=335$ K) and the copper does have an oxygen in the apical position albeit at a large distance of 2.511 Å. In $AgCuVO_4$ was observed that the strength of the exchange and the existence of interchain exchange paths leads to a three-dimensional ordered ground state near $T_N=2.5$ K. It is interesting to note that here no long range ordering is detected down to the lowest measured temperature This results from the moderate strength of the intra-chain exchange and the absence of super-exchange paths to magnetically connect the chains, making $CaCuGeO_4 \cdot H_2O$ a strong candidate for a one-dimensional ground state system.

The susceptibility of (**2**) was successfully fitted using the Baker expression [21,22], in agreement with the observed ferromagentic nearest-neighbor interaction. However, these data were fitted only down to 8 K, since below this temperature long range interactions are observed arising from interchain correlations between the ferromagnetic chains, and the Baker model, applied here, does not account for this extra interaction.

In compound (**2**), the small value of θ_p makes the visualization of the susceptibility as χT as a function of temperature, particularly useful. The data in that form, as well as the fits of both samples to the appropriate model, are presented in Fig. 6. As expected, the plot of χT as a function of temperature of (**1**) shows a monotonic decrease with decreasing temperature, which is a signature of a strong antiferromagnetic arrangement between ions along the chain. However, for (**2**) χT has a broad minima, around 70 K followed by a peak at 8 K. The almost linear decrease of χT from high temperatures down to 70 K is due to the temperature-independent contribution, the slow increase of χT below this temperature is a clear signature of ferromagnetic interactions along the chain. This increase is suppressed at about 8 K, when a peak is observed and an abrupt reduction in χT signals at the onset of antiferromagnetic interchain interactions. Interestingly, the edge sharing Cu(II) chain present in this compound is very similar to the ones existing in quite notable examples in chain magnetism: one is the prototypical $CuGeO_3$, where a Bonner–Fisher behavior with $J=-88$ K is followed by a Spin–Peierls transition at $T_{SP}=14$ K, this was the first example of a Spin–Peierls transition detected in an inorganic system [9]. Another compound with a similar edge sharing chain arrangement is $LiCuVO_4$, a quasi-one-dimensional

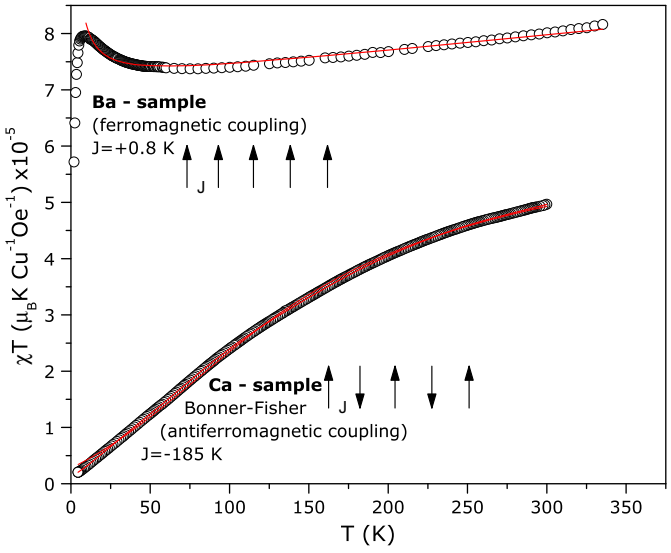

Fig. 6. Susceptibility times temperature as a function of temperature for both Ba- and Ca-samples. Red lines represent the fits to the model described in the text. (For interpretation of the references to color in this figure caption, the reader is referred to the web version of this article.)

helimagnet with a nearest-neighbour ferromagnetic, next-nearest-neighbour frustrated interaction [25], this compound was later found to exhibit a ferroelectric transition induced by the incommensurate magnetic ordering [26]. What sets these two examples in contrast with (**2**) is that while in the $CuGeO_3$ and $LiCuVO_4$ the equatorial square-planes that make up the chain are coplanar, and therefore maximize the magnitude of the exchange, resulting in $J=-88$ K for the former and $J=42$ K for the latter, in the present case there is a significant canting of these planes of 158°, as is schematically represented in the inset of Fig. 4. This extra distortion, significantly weakens the copper-copper magnetic interaction along the chain, resulting in $J\sim 0.8$ K and therefore precluding the observation of any exotic cooperative phenomena at experimentally accessible temperatures.

4. Conclusions

Two new alkaline earth copper germanate compounds were synthesized through hydrothermal synthesis. The calcium sample is layered with a network of hydrogen bonds connecting the layers, while the barium sample consists of a three-dimensional framework with octahedral and tetrahedral germanium and copper in a highly distorted octahedral environment. For both samples the copper ions form chains: in the calcium compound by corner sharing and in the barium case an edge sharing one. This leads to a dramatically different magnetic behavior. The susceptibility of calcium sample was fitted with a Bonner–Fisher type formulation (antiferromagnetic), without three-dimensional ordering, making this system particularly promising for the study of systems with one-dimensional magnetic ground state; while the barium sample behaves as a one-dimensional ferromagnet, with the χT plot signaling the onset of interchain interaction at 8 K.

Acknowledgments

P.B. thanks FCT and FEDER (QREN-COMPETE-FCOMP 01-0124 FEDER-007461) for funding the Project PTDC/QUI/72584/2006 and collaboration project between Portugal and Brazil FCT/CAPES/2011/2012. Research at ORNL was conducted at the Quantum Condensed Matter Division and the CNMS, which are sponsored at ORNL by the Office of Basic Energy Sciences, U.S. DOE. The ORNL is managed by UT-Battelle, LLC for the U.S. DOE under Contract no. DE-AC05-00OR22725. M.S.R. acknowledge Brazilian agencies: CAPES, CNPq, FAPERJ and PROPPi-UFF.

Appendix A

Further details of the crystal structure investigation can be obtained from the Fachinformationszentrum (FIZ) Karlsruhe, D-76344 Eggenstein-Leopoldshafen, Germany (fax: +49 7247/808 666; e-mail: crysdata@fiz-karlsruhe.de) on quoting the depository numbers CSD-424817 for (**1**) and CSD-424818 for (**2**).

Appendix B. Supplementary data

Supplementary data associated with this article can be found in the online version at http://dx.doi.org/10.1016/j.jssc.2012.09.006.

References

[1] A.K. Cheetham, G. Ferey, T. Loiseau, Angew. Chem. Int. Ed. 38 (1999) 3268–3292.
[2] R.M. Barrer, Hydrothermal Chemistry of Zeolites, Academic Press, 1989.
[3] S.T. Wilson, B.M. Lok, C.A. Messina, T.R. Cannan, E.M. Flanigen, J. Am. Chem. Soc. 104 (1982) 1146–1147.
[4] J. Rocha, M.W. Anderson, Eur. J. Inorg. Chem. (2000) 801–818.
[5] M. O'Keeffe, O.M. Yaghi, Chem. Eur. J. 5 (1999) 2796–2801.
[6] K.E. Christensen, Crystallogr. Rev. 16 (2010) 91.
[7] X.H. Bu, P.Y. Feng, G.D. Stucky, Chem. Mater. 12 (2000) 1811–1813.
[8] N.N. Julius, A. Choudhury, C.N.R. Rao, J. Solid State Chem. 170 (2003) 124–129.
[9] M. Hase, I. Terasaki, K. Uchinokura, Phys. Rev. Lett. 70 (1993) 3651–3654.
[10] Y. Sasago, M. Hase, K.U. Chinokura, M. Tokunaga, N. Miura, Phys. Rev. B 52 (1995) 3533–3539.
[11] I. Tsukada, J. Takeya, T. Masuda, K. Uchinokura, Phys. Rev. B 62 (2000) R6061–R6064.
[12] A.M. Souza, D.O. Soares-Pinto, R.S. Sarthour, I.S. Oliveira, M.S. Reis, P. Brandao, A.M. dos Santos, Phys. Rev. B 79 (2009) 54408–54412.
[13] M.A. Monge, E. Gutierrez-Puebla, C. Cascales, J.A. Campa, Chem. Mater. 12 (2000) 1926–1930.
[14] Y.-F. Li, D.-P. Li, C.-L. Shi, Y.-S. Hu, L. Jin, Acta Crystallogr. Sect. E 65 (2009) I27–U149.
[15] G.M. Sheldrick, SHELXL-97, Computer Program for Crystal Structure Refinement, 1987.
[16] G.M. Sheldrick, Acta Crystallogr. Sect. A 64 (2008) 112–122.
[17] K. Momma, F. Izumi, J. Appl. Crystallogr. 41 (2008) 653–658.
[18] J.B. Goodenough, J. Phys. Chem. Solids 6 (1958) 286.
[19] J. Kanamori, J. Phys. Chem. Solids 10 (1959) 87.
[20] J.C. Bonner, M.E. Fisher, Phys. Rev. A–Gen. Phys. 135 (1964) A640–A658.
[21] G. Baker, G. Rushbrooke, H. Gilbert, Phys. Rev. 135 (1964) A1272.
[22] L. Thompson, S. Tandon, F. Lloret, J. Cano, M. Julve, Inorg. Chem. 36 (1997) 3301.
[23] O. Kahn, Molecular Magnetism, Wiley VCH Publishers, 1993.
[24] A. Moeller, M. Schmitt, W. Schnelle, T. Foerster, H. Rosner, Phys. Rev. B 80 (2009) 125106.
[25] M. Enderle, C. Mukherjee, B. Fak, R. Kremer, J. Broto, H. Rosner, S. Drechsler, J. Richter, J. Malek, A. Prokofiev, W. Assmus, S. Pujol, J. Raggazzoni, H. Rakoto, M. Rheinstadter, H. Ronnow, Europhys. Lett. 70 (2005) 237–243.
[26] Y. Naito, K. Sato, Y. Yasui, Y. Kobayashi, Y. Kobayashi, M. Sato, J. Phys. Soc. Jpn. 76 (2007).